The versatile molecular complex component LC8 promotes several distinct steps of flagellar assembly

Anjali Gupta,[1] Dennis R. Diener,[2] Priyanka Sivadas,[1] Joel L. Rosenbaum,[2] and Pinfen Yang[1]

[1]Department of Biological Sciences, Marquette University, Milwaukee, WI 53201
[2]Department of Molecular, Cellular, and Developmental Biology, Yale University, New Haven, CT 06520

LC8 is present in various molecular complexes. However, its role in these complexes remains unclear. We discovered that although LC8 is a subunit of the radial spoke (RS) complex in *Chlamydomonas* flagella, it was undetectable in the RS precursor that is converted into the mature RS at the tip of elongating axonemes. Interestingly, LC8 dimers bound in tandem to the N-terminal region of a spoke phosphoprotein, RS protein 3 (RSP3), that docks RSs to axonemes. LC8 enhanced the binding of RSP3 N-terminal fragments to purified axonemes. Likewise, the N-terminal fragments extracted from axonemes contained LC8 and putative spoke-docking proteins. Lastly, perturbations of RSP3's LC8-binding sites resulted in asynchronous flagella with hypophosphorylated RSP3 and defective associations between LC8, RSs, and axonemes. We propose that at the tip of flagella, an array of LC8 dimers binds to RSP3 in RS precursors, triggering phosphorylation, stalk base formation, and axoneme targeting. These multiple effects shed new light on fundamental questions about LC8-containing complexes and axoneme assembly.

Introduction

LC8 is a small, yet vital, protein in a wide spectrum of protein complexes. This 10-kD molecule functions as a dimer (Liang et al., 1999) with two identical grooves formed at the dimeric interface. The grooves bind to a 12-aa region in >100 proteins (Lo et al., 2001; Rodríguez-Crespo et al., 2001; Navarro-Lérida et al., 2004), including apoptotic factor BimL (Puthalakath, et al., 1999), intermediate chains (ICs) of dynein motors (Lo et al., 2001), myosin V (Espindola et al., 2000), the membrane-associated protein Bassoon (Fejtova, et al., 2009), and a phosphoprotein encoded by a viral transcript (Tan et al., 2007). Although the majority of LC8 target proteins contain one LC8-binding site, there are a few exceptions that harbor two (Lo et al., 2005; Rompolas et al., 2007), or multiple, sites aligned in tandem (Stelter et al., 2007; Fejtova et al., 2009). Some of these target proteins simply form heteromers with LC8, whereas the others exist in macromolecular complexes with multiple subunits (King and Patel-King, 1995; Puthalakath, et al., 1999; Yang et al., 2001; Pfister et al., 2006). Appreciation of LC8's impact is just beginning. Structural studies of dynein ICs suggest that the two grooves of an LC8 dimer bind both chains in a dimer to enhance the stability of a molecular complex (Williams et al., 2007). In other cases, LC8 dimers bind to disordered regions in target proteins, and the binding promotes their refolding (Barbar, 2008). In one instance, a stack of five LC8 dimers associates with two Nup159 chains in the nuclear pore complex to form a rod-shaped structure (Stelter et al., 2007).

However, it is not clear how to use these models to explain the phenotypes of *Chlamydomonas* LC8 mutants (Yang et al., 2009). LC8 is present in axonemal and cytoplasmic dyneins and the radial spoke (RS) complex in eukaryotic cilia and flagella (King and Patel-King, 1995; Yang et al., 2001, 2009; Kamiya, 2002). Consistent with the models that implicate LC8 in the key structure of molecular complexes, these flagellar complexes are absent or drastically reduced in the flagella of the LC8-null strains *fla14-1* and *fla14-2* (Pazour et al., 1998). Yet, these complexes are affected differently in the allelic mutant *fla14-3* (Yang et al., 2009). In this strain, because of a loss of the primary stop codon of the LC8 gene, 23 aa are appended to the absolutely conserved C terminus, distant from the target-binding grooves. The axonemal dynein motors appear largely unaffected,

Correspondence to Pinfen Yang: pinfen.yang@marquette.edu

Abbreviations used in this paper: AH, amphipathic helix; CSC, CaM- and spoke-associated complex; IC, intermediate chain; IFT, intraflagellar transport; N-DRC, nexin–dynein regulatory complex; NTA, nitrilotriacetic acid; PMM, paromomycin; RS, radial spoke; RSP, radial spoke protein; WT, wild type.

The Rockefeller University Press $30.00
J. Cell Biol. Vol. 198 No. 1 115–126
www.jcb.org/cgi/doi/10.1083/jcb.201111041

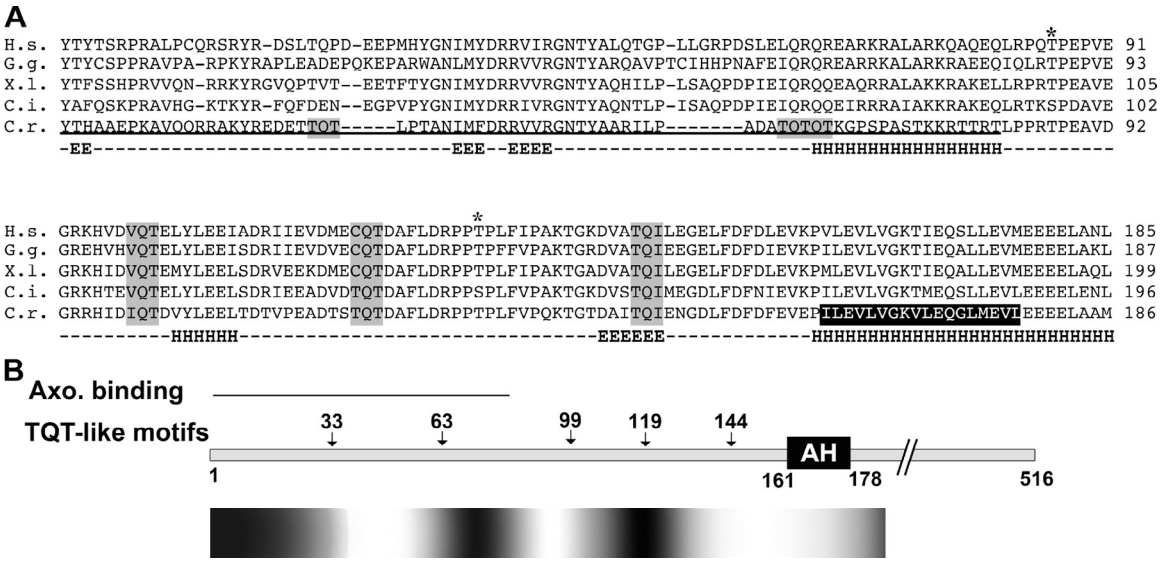

Figure 1. **Sequence analysis of RSP3.** (A) Sequence alignment of RSP3 orthologs. The TQT-like LC8-binding motifs (gray boxes) are adjacent to the axoneme-binding region (underlined) near the N terminus and upstream to the AH that binds the RIIa domain (black box at aa 161–178). As in many LC8-binding sites, in some of these sites in RSP3, T is replaced by aa residues with similar properties. Asterisks represent the predicted ERK1/2 phosphorylation sites. The secondary structure of the *C. reinhardtii* RSP3 sequence was predicted by the Jpred program. H.s., *Homo sapiens*; G.g., *Gallus gallus* (chicken); X.l., *Xenopus laevis*; C.i., *Ciona intestinalis*; C.r., *Chlamydomonas reinhardtii*; H, α helix; E, β strand; −, random coil. (B) Schematic depicting the region containing the TQT-like motifs in full-length *Chlamydomonas* RSP3. The tertiary structure was predicted using the Regional Order Neural Network Disorder Prediction tool. Arrows mark the position of the putative LC8-binding motifs. The white area represents <50% disorder; the black area represents >50% disorder. Axo, axoneme.

suggesting that the target-binding grooves are not substantially disturbed by the C-terminal extension. However, the RSs in *fla14-3* axonemes are severely defective; they are less abundant and readily dissociate upon extraction, unlike the intact wild-type (WT) RS. In addition, a phosphoprotein in the RS, RS protein 3 (RSP3), migrates faster in SDS-PAGE like hypophosphorylated RSP3 (Huang et al., 1981; Piperno and Luck, 1981; Segal and Luck, 1985; Yang et al., 2009). The contrast of severe and various defects in the RS caused by LC8's extended C-terminal tail, relative to subtle changes in axonemal dyneins, suggests that the roles of LC8 in these complexes are different.

In *Chlamydomonas*, the RS is critical for flagellar beating and appears as a T or a drum stick, comprised of LC8, RSP3, and at least 17 other distinct RSPs (Huang et al., 1981; Piperno and Luck, 1981; Yang et al., 2001, 2006; Patel-King et al., 2004; Pigino et al., 2011). RSPs are synthesized in the cell body, and some of them assemble into a precursor complex with a 12S sedimentation coefficient (Qin et al., 2004; Diener et al., 2011). Diverse evidence suggests that the 12S complexes are delivered to the flagellar compartment and moved by the kinesin-driven anterograde intraflagellar transport (IFT) to the flagellar tip, where they are converted into mature 20S RSs, and integrated into the nine microtubule outer doublets (Johnson and Rosenbaum, 1992; Qin et al., 2004). The severe deficiencies of the RS in LC8 mutants suggest that LC8 plays a critical role in this complicated assembly process.

Here, we report that multiple LC8 dimers bind to RSP3 in the flagellar compartment, promoting RSP3 phosphorylation. The LC8–RSP3 complex is critical for at least two aspects of assembly: the forming of the spoke stalk and docking the stalk to RS-docking complexes. Understanding the multiplex effects that LC8 exerts on RSP3 will help elucidate events of RS assembly and how LC8 might function in other complexes.

Results

LC8-binding motifs are present at the N-terminal region of RSP3

LC8 is a component of the mature multisubunit RS (Yang et al., 2001), but its binding partner has not been identified. Therefore, we searched all the RSP sequences for LC8-binding motifs. A fraction of LC8-binding sequences have a [(K/R)XTQT] motif (Lo et al., 2001); however, in many cases, the basic residue is absent, and the T residues can be replaced by noncharged aa like S, I, V, or C (Jaffrey and Snyder, 1996; Rodríguez-Crespo et al., 2001; Stelter et al., 2007). RSP3 is the only RSP to contain a TQT or TQT-like motif, and, in fact, the *Chlamydomonas* RSP3 N-terminal 160 aa contain five such motifs spaced at 17–31-aa intervals (Fig. 1 A, shaded residues). Of these five motifs, the first two are located within the axoneme-binding region of RSP3 (Fig. 1 B) and are not present in RSP3 homologs from vertebrates. In contrast, the last three motifs are conserved in vertebrates; the central Q is retained among all orthologs, whereas the flanking residues are either T or residues present in confirmed LC8-binding motifs. As proposed earlier for LC8-binding regions (Barbar, 2008), sequence analysis predicts that the secondary structure of $RSP3_{1–160}$ is primarily comprised of random coils, lacking extended α helices or β strands (H and E in Fig. 1 A) or ordered tertiary structure (Fig. 1 B, gradient bar), whereas the rest of the RSP3 polypeptide is largely helical (unpublished data).

Finally, like many LC8-binding proteins, RSP3 exists in RSs as a homodimer (Wirschell et al., 2008). Based on these observations, we postulate that the N-terminal region of an RSP3 dimer associates with at least three LC8 dimers.

Trypsin-digested spoke complexes contain both RSP3 N-terminal fragments and LC8

To test for interactions between LC8 and the RSP3 N-terminal region in situ, we treated axonemes with limited trypsin proteolysis. The base of the spoke should contain the axoneme-binding RSP3 N-terminal fragment (Diener et al., 1993), which we propose binds LC8. Axonemes of *pf28pf30* cells, which lack LC8-containing dyneins, were treated with trypsin and extracted with KI buffer to remove the remaining RSs. The extracted RSs were analyzed on immunoblots of native (Fig. 2 A) and denaturing (Fig. 2 B) gels probed with a pan-RSP3 antibody that recognizes the first 300 aa of *Chlamydomonas* RSP3. Two major RS complexes, both smaller than untreated RSs, were identified on native gels of the extract from the axonemes treated with trypsin at a ratio of 100:1 by weight (Fig. 2 A). These subcomplexes became diminished if the trypsin concentration was doubled (Fig. 2 A, third lane), so a 100:1 axoneme/trypsin ratio was used for subsequent experiments. After SDS-PAGE, RSP3 was detected as 30- and 20-kD fragments (Fig. 2 B, top), whereas LC8 remained intact (Fig. 2 B, bottom). Therefore, limited proteolysis of axonemes produced subcomplexes of RSs containing N-terminal fragments of RSP3.

To determine whether LC8 was present in the RS subcomplexes containing the N-terminal fragment of RSP3, lanes excised from the native gel were subjected to SDS-PAGE (Fig. 2 C, schematic). Proteins that comigrate on the native gel will align vertically in the denaturing gel. To visualize the relevant polypeptides, the blot from the resulting 2D gel was probed for LC8 (Fig. 2 C, top) and then RSP3 (asterisks in Fig. 2 C, middle). As proposed, LC8 migrated as two major spots that aligned predominantly with the 30-kD and, to a lesser extent, the 20-kD RSP3 fragment. To better delineate the boundaries of the two RSP3 fragments, the blot was reprobed for RSP11 (Fig. 2 C, bottom), which binds to the amphipathic helix (AH) adjacent to the last LC8-binding motif (Fig. 2 D, AH). Two RSP11 spots of similar size and intensity (Fig. 2 C, lines) comigrated with RSP3 and LC8, indicating that the 30- and 20-kD RSP3 fragments include the AH (aa 161–178). These results suggest that the 30-kD fragment binds more LC8 than the 20-kD fragment (Fig. 2 D), consistent with the fragments differing in their N-terminal end, which includes multiple LC8-binding motifs near the region that dock the RS to outer doublets.

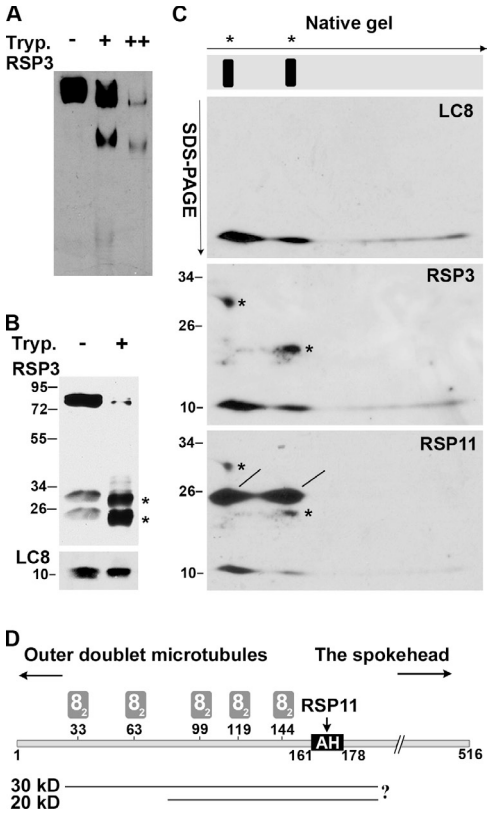

Figure 2. **Comigration of LC8 and the RSP3 N-terminal proteolytic fragments in electrophoresis.** (A–C) Native gel electrophoresis (A), SDS-PAGE (B) and native/SDS-PAGE 2D electrophoresis (C) of the KI extract from *pf28pf30* axonemes that were pretreated with the buffer only or with trypsin (Tryp.) at the ratio of 100:1 (+) or 100:2 (++) by weight. The blots were probed sequentially for LC8, the RSP3 N-terminal region, and RSP11, which contains an RIIa domain that binds to the AH adjacent to the last LC8-binding site. RS subcomplexes containing RSP3 N-terminal fragments were resolved into two particles in the native gel (A) and depicted as two lines in a gel strip schematic in C. Arrows indicate the directions of electrophoresis. The digested RSP3 N-terminal fragments migrated as ~30- and 20-kD fragments in SDS-PAGE (B and C, asterisks). In the 2D gel, LC8 and RSP11 (lines) aligned vertically with the two RS subcomplexes. The LC8 spot that aligned with the 30-kD RSP3 fragment appeared more abundant than the LC8 aligned with the 20-kD RSP3 fragment; the two RSP11 spots appeared equally abundant. (D) Schematic depicting the predicted positions of the two proteolytic fragments near the RSP3 N terminus, relative to the binding sites for LC8 dimers (gray rectangles, 8_2), outer doublets, and the spokehead. The prediction was based on Western blots, the size of proteolytic fragments, and trypsin cleavage sequences. The actual cleavage sites were not mapped (indicated by a question mark).

Direct interaction of recombinant LC8 and RSP3$_{1-160}$

To test for direct interactions between LC8 and RSP3, we separately expressed in bacteria His-tagged LC8 and S-tagged RSP3$_{1–160}$, which includes all five potential LC8-binding motifs. When Ni–nitrilotriacetic acid (NTA) was used to purify His-tagged LC8 from a mixture of the two bacterial extracts, RSP3$_{1–160}$ was copurified with LC8 (Fig. 3 A, arrowhead), suggesting that these proteins directly bind to each other. This result was upheld in the reciprocal experiment: S agarose also brought down both S-tagged RSP3$_{1–160}$ and His-tagged LC8 from the mixed extracts (Fig. 3 B, arrowhead). Controls testing each extract separately demonstrated that the S-tagged RSP3 alone has a low affinity for Ni-NTA, and the His-tagged LC8 has a low affinity for S agarose (compare the last three lanes in Fig. 3, A and B). To estimate the relative stoichiometry of these two molecules in the complex, we measured the Coomassie-stained bands of LC8 and RSP3 in the S agarose–purified sample because LC8 in the extract appeared to be in excess (Fig. 3 B). The ratio of mean densities divided by the molecular masses of each protein led to an approximate stoichiometric ratio of 1:3 for RSP3$_{1–160}$/LC8. These results suggest that in vitro, each dimeric RSP3$_{1–160}$ directly binds at least three LC8 dimers.

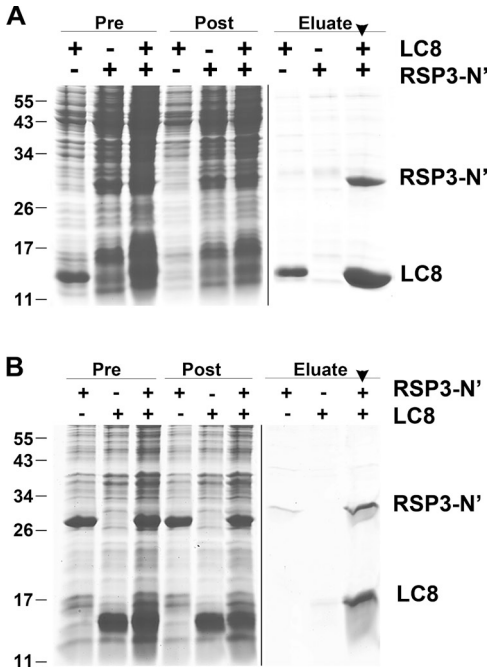

Figure 3. **Copurification of recombinant LC8 and RSP3$_{1–160}$.** (A and B) Ni-NTA (A) and S tag (B) affinity purification of the bacterial extracts containing His-tagged LC8 or S tag RSP3$_{1–160}$ or the mixture of both extracts. Protein samples were fractionated by SDS-PAGE and stained with Coomassie blue. Both fusion proteins in the extract mixtures were copurified by both matrices (arrowhead in eluate lane). The aberrant migration of the S tag eluate was a result of the high salt concentration in the elution buffer. Pre, bacterial extract; Post, flow through. Molecular mass is indicated in kilodaltons.

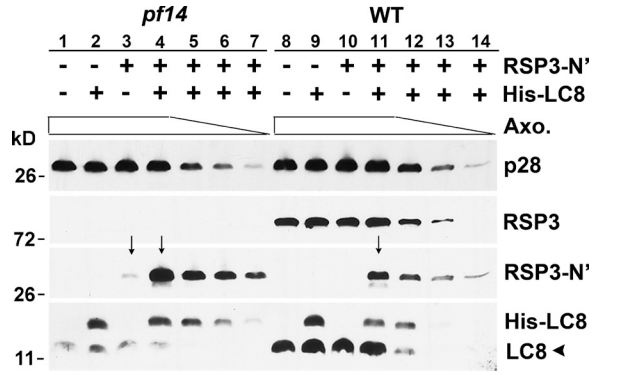

Figure 4. **LC8 enhances the binding of RSP3 N-terminal fragment to the spokeless *pf14* axonemes.** Bacterial extract containing RSP3$_{1–160}$, His-LC8, or both was incubated with different amounts (clear bar) of axonemes from *pf14* or the WT strain. The axoneme (Axo.) pellets were fractionated by SDS-PAGE, and the Western blots were probed as indicated. *pf14* axonemes pulled down more RSP3 fragments than WT axonemes (compare lanes 4 and 11, arrows), whereas addition of His-tagged LC8 greatly increased the amount of RSP3 bound by *pf14* axonemes (compare lanes 3 and 4, arrows). A subunit of I2 and I3 inner dyneins, p28, was used to indicate the amounts of axonemes (clear bar). Endogenous untagged LC8 (arrowhead) was substantially less abundant in *pf14* than WT.

LC8 enhances the reconstitution of RSP3$_{1–160}$ to the spokeless axoneme

To test whether binding of LC8 promotes RSP3 docking to the axoneme, the RSP3$_{1–160}$-containing bacterial extract was mixed with different amounts of *pf14* axonemes, which lack RSP3 in the presence or absence of the His-LC8–containing bacterial extract (Fig. 4, lanes 1–7). WT axonemes in which all or most of the RSP3-binding sites are occupied were used as a control (Fig. 4, lanes 8–14). After incubation, axonemal pellets were analyzed by Western blots for bound RSP3$_{1–160}$ and LC8. The quantity of axonemes was reflected by p28, a dynein subunit that is normal in axonemes from both strains (LeDizet and Piperno, 1995). In the presence of LC8, the amount of RSP3$_{1–160}$ bound to the *pf14* axonemes was demonstrably greater than the sample without LC8 as well as to the equivalent samples using WT axonemes (compare arrows in Fig. 4, lanes 3 and 4 and lanes 4 and 11). Collectively, Figs. 3 and 4 show that LC8–RSP3 interactions promote the specific binding of RSP3$_{1–160}$ to the spokeless axonemes.

Interestingly, significant amounts of recombinant LC8 itself bind to axonemes (Fig. 4, lanes 2 and 9), and LC8 also enhances the nonspecific association of RSP3 with WT axonemes (Fig. 4, compare lane 10 and 11). These may be related to the promiscuity of LC8 and suggest that the interactions of LC8 and its intended target proteins are controlled (see following section). It is worthwhile to point out that although axonemes have five dyneins that contain LC8 for every pair of RSs (Kamiya, 2002; DiBella et al., 2005; Pfister et al., 2006), the endogenous LC8 (Fig. 4, arrowhead) present in the spokeless *pf14* axonemes is about equivalent to that in one half as many WT axonemes (Fig. 4, bottom). Thus, each RS apparently contains multiple LC8 dimers.

Homodimerization of the RSP3 N-terminal region

High-resolution electron micrographs suggest that two monomeric target proteins dimerize and align in parallel while associating with a stack of LC8 dimers (Stelter et al., 2007). To test whether RSP3$_{1–170}$ undergoes such dimerization in vivo, we expressed RSP3$_{1–170}$ with a three-Cys tag at the C terminus in the RSP3 mutant *pf14*. We envisioned that if the LC8-binding fragments are closely aligned with each other, the adjacent Cys residues could form intermolecular disulfide bonds in an oxidative environment. Interestingly, when analyzed by routine SDS-PAGE (140 mM β-mercaptoethanol), axonemes from RSP3$_{1–170}$-Cys strains displayed two groups of bands: one set of bands appeared as a doublet of 25 and 30 kD (Fig. 5 A, arrows), whereas the other was a thick band migrating at 50–55 kD (Fig. 5 A, asterisk). The smaller double bands may be differentially phosphorylated monomers of RSP3$_{1–170}$-Cys, as in vitro phosphorylation of human RSP3 showed that the first 170 aa contain two phosphorylation sites (Fig. 1; Jivan et al., 2009). The 50–55-kD bands appear to be a dimer of RSP3$_{1–170}$-Cys, broadened by phosphorylation. These upper bands were absent when the sample was fully reduced with 420 mM β-mercaptoethanol (Fig. 5 A, right lane), indicating they were indeed dimeric RSP3$_{1–170}$-Cys cross-linked by disulfide bonds at the C terminus.

To test whether the dimerization is inherent to RSP3$_{1–170}$ or induced by the Cys tag, the terminal Cys residues of RSP3$_{1–170}$-Cys were replaced with three HA epitopes and 12 His residues (RSP3$_{1–170}$-HAHis). SDS-PAGE analysis of axonemes from

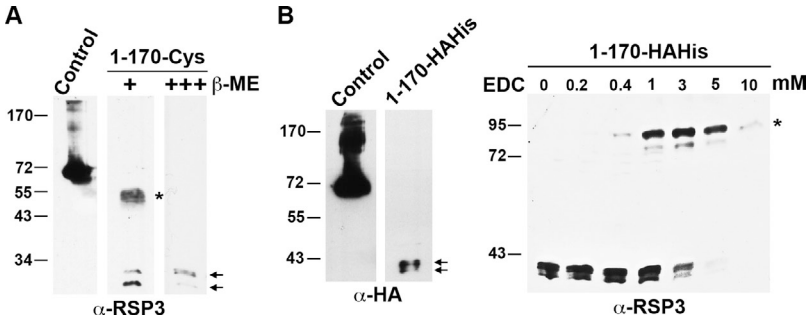

Figure 5. **RSP3$_{1–170}$ in axonemes exists as homodimers.** (A and B) RSP3 and HA Western blots of the axonemes from the strains expressing RSP3$_{1–170}$ that has a C-terminal tag containing three Cys residues (A) or three HA epitopes and 12 His residues (B). Monomeric RSP3$_{1–170}$ migrated as double bands (arrows). A portion of Cys-tagged RSP3$_{1–170}$ migrated as the polypeptides twice the size of monomers (A, asterisk) in the presence of 140 mM β-mercaptoethanol (β-ME). The putative dimer bands were absent when the reducing agent was threefold as concentrated. The dimer bands were not present in RSP3$_{1–170}$-HAHis axonemes (B, left) unless they were treated with the zero-length cross-linker EDC (asterisk in B, right). The amount of RSP3$_{1–170}$ in the axonemes was small compared with the control sample of axonemes from cells expressing HAHis-tagged RSP3$_{\Delta171–244}$ lacking aa 171–244. Molecular mass is indicated in kilodaltons.

cells expressing this construct revealed a doublet of RSP3$_{1–170}$-HAHis monomers at 38–42 kD, but the dimeric bands were absent (Fig. 5 B, left). However, dimeric RSP3$_{1–170}$-HAHis could be formed by treating the axonemes with the zero-length cross-linker (EDC [1-ethyl-3-(3-dimethylaminopropyl) carbodiimide]; Fig. 5 B, asterisk). These results indicate that the RSP3$_{1–170}$-HAHis forms an 84-kD dimer in the axoneme, as expected of LC8 target polypeptides. Note that amounts of Cys- or HAHis-tagged RSP3$_{1–170}$ are significantly less abundant than RSP3$_{\Delta171–244}$ (Fig. 5, control), which contains the entire RSP3 except for aa 171–244. Thus, an additional sequence beyond the LC8-binding region may improve the assembly of RSP3 polypeptides in axonemes.

RSP3$_{1–178}$ complex contains LC8 and putative RS-docking proteins

The RSP3 N terminus is implicated in docking RSs to axonemes (Diener et al., 1993); furthermore, in a protein blot overlay, RSP3, used as a ligand, binds to a subunit of the CaM- and spoke-associated complex (CSC) that was pulled down with the intact RS complexes by CaM immunoprecipitation (Dymek and Smith, 2007). To test whether the LC8–RSP3 complex associates with the CSC molecules that may dock RSs to axonemes, we pulled down RSP3 N-terminal fragments from the axonemal extract. Because of the low abundance of RSP3$_{1–170}$, we used the axonemes from *pf14* transformants expressing RSP3$_{1–178}$-HAHis, which is abundant and contains the complete 18-aa AH (aa 160–178; Fig. 1 B, AH) that anchors the RIIa domain. The axonemes were extracted with KI buffer, and the extracts were incubated with Ni-NTA. As expected, Western blots and protein gels showed that in addition to RSP3$_{1–178}$, Ni-NTA specifically brought down LC8 and the RIIa-containing RSP7 and RSP11 (compare pre, post, and eluate of 1–178 samples in Fig. 6, A and B). In addition, Ni-NTA also brought down CaM-IP2, -IP3, and -IP4 (Fig. 6 B, dots) in the CSC. These proteins were not brought down in the *pf14* control. Curiously, CaM was not in the pull-down. As the RS in RSP3$_{1–178}$ strain lacks the spoke-head region, this result indicates that the CSC is in the vicinity of the spoke base and the axoneme-binding region of RSP3.

Interestingly, the silver-stained gel showed that Ni-NTA also specifically brought down an unknown 85-kD protein (Fig. 6 B, arrow) with similar stoichiometry as CaM-IP3 and -IP4 (Fig. 6 B, dots). Liquid chromatography–tandem mass spectrometry of this purified band revealed eight peptide sequences (Table 1) from the flagella-associated protein FAP206 that was initially recovered by the flagellar proteomic study

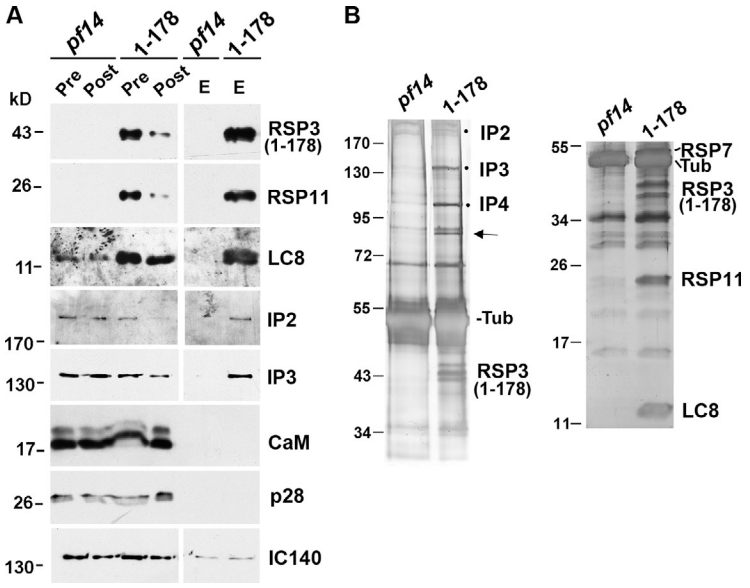

Figure 6. **The pull-down of RSP3$_{1–178}$ contains LC8, RSPs, and putative RS-docking proteins.** (A and B) Western blots (A) and silver-stained protein gels of the Ni-NTA pull-down (B) from the KI axonemal extracts of *pf14* and the *pf14* transformant that expresses RSP3$_{1–178}$-HAHis. The RSPs in the RSP3$_{1–178}$ pull-down were LC8 and the RIIa domain–containing RSP7 (B, right) and RSP11 (A and B, right blots). An unknown 85-kD doublet (arrow) and CaM-IP2, -IP3, and -IP4 (dots) in the CSC were also in the pull-down but were scarce or undetectable in the pull-down from *pf14*. CaM and IC140 in the inner dynein arm I1 were not pulled down appreciably. CaM-IP4 was identified based on its copurification with CaM-IP2 and CaM-IP3 and its molecular mass. Pre, axonemal extract; Post, flow-through; E, eluate; Tub, tubulin.

Table 1. **Peptide sequences of the 85-kD axonemal protein copurified with RSP3$_{1–178}$-HAHis**

Scan no.	Sequence
7	LTQLAELAR
6	VDPYVVAYVTSLEDAR
5	AFLSDPAAVLAGVAAAVAR
4	VYGFSSNADMR
3	GALQSLVPDVSLK
3	AALESVFPVSAVSR
1	AGAVSSEAVAAIGGYVAGLVGDAR
1	FVTLAEGER

The protein band of the Ni-NTA pull-down sample in a silver-stained gel was excised, and the peptide sequences were revealed by liquid chromatography–tandem mass spectrometry. All correspond to flagella-associated protein FAP206.

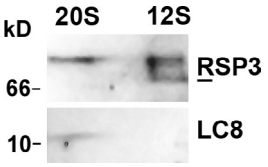

Figure 7. **LC8 is undetectable in the RS precursors.** The flagellar membrane matrix from *pf28pf30*, which lacks LC8-containing axonemal dyneins, was first fractionated through a sucrose gradient. The 20S and 12S fractions were subjected to further purification through a MonoQ column. The protein blots of RS-positive fractions from the anionic chromatography were probed for RSP3 and LC8. LC8 was detectable in the purified 20S complex but not in the 12S complex. RSP3 was used as a loading control. A fraction of the 12S RSP3 migrated faster (line) than the 20S RSP3.

(Pazour et al., 2005) and was recently found reduced in spokeless *pf14* axonemes (Lin et al., 2011). Like RSPs (Yang et al., 2001), FAP206 is resistant to NaCl extraction and is enriched in the extracted axonemal pellet (Pazour et al., 2005). Although the initial FAP206 gene model predicted a 309-aa protein, the 85-kD molecular mass observed by SDS-PAGE is consistent with the 712-aa gene model in the *Chlamydomonas* v.4 genome. A BLASTP search showed that FAP206 shares extensive sequence homology with human C6ORF165 (NCBI Protein database accession no. NP_001026913) and other orthologs only expressed by organisms with motile cilia and flagella. Consistent with its presence in flagella, the expressed sequence tags of C6ORF165 are particularly enriched in testis (National Center for Biotechnology Information Expressed Sequence Tags database).

LC8 is not detectable in the 12S RS precursor

About half of the RSPs are known to assemble in the cell body to form a 12S complex that is transported into the flagella (Diener et al., 2011). It was proposed that in the flagella, the 12S complex dimerizes and combines with the other RSPs to form the mature 20S RS. Because the 12S complex contains a dimer of RSP3, we expected that it would also contain LC8; however, this was not the case. Soluble 12S and 20S RSP complexes were purified from flagella of *pf28pf30*, which lack the LC8-containing axonemal dyneins. Immunoblot analysis of these complexes revealed that LC8 was present in the 20S complex but undetectable in the 12S complex (Fig. 7). This result suggests that LC8 is not involved in formation of the RSP3 dimer, assembly of the 12S complex, or its transport into the flagella. Work with *fla14* also supports this conclusion: though *fla14* lacks LC8, the 12S and 20S RS complexes are present in the soluble fraction of its flagella (Qin et al., 2004).

Perturbation of RSP3's LC8-binding motifs results in hypophosphorylated RSP3 and defective associations among RS, LC8, and outer doublets

To test the importance of LC8–RSP3 interactions in vivo, we altered the putative LC8-binding sites in full-length RSP3-HA-His genomic constructs and expressed these proteins in *pf14*. Mutations were made in either the first two sites (1–2), the last three sites (3–5), or all five sites (1–5). In strains labeled AN, one T residue in the TQT-like motif was replaced by A, and Q was replaced by N. Because complete replacement of the TQT-like motif is necessary to perturb consecutive LC8-binding sites in BIG1 (Fejtova et al., 2009), we also generated AAA strains in which all three TQT-like residues were replaced by A. All constructs contained an antibiotic expression cassette and were transformed into the *pf14* strain. For each construct, ∼50 antibiotic-resistant transformants were screened microscopically for motility. All constructs were capable of restoring motility to the paralyzed flagella of *pf14*, albeit to different degrees. The motility phenotypes are summarized in Table 2. Therefore, the putative LC8-binding sites are involved, but not essential, in generating flagellar motility.

Swimming by all AN strains and the 1-2AAA strains was indistinguishable from the control transformed with the WT gene (Fig. 8, A and B). The 3-5AAA and 1-5AAA strains exhibited a phenotype common to mutants with mild RS deficiencies: ∼50% of the cells in liquid cultures swam, but the remainders were immotile, with paralyzed or twitching flagella of largely asymmetric waveform (Gaillard et al., 2006; Yang and Yang, 2006; Wei et al., 2010). The swimmers easily became attached to the glass surface during video microscopy, and their flagella lost synchrony frequently, leading to irregular trajectories (Fig. 8, C and D), indicating that the motility is partially restored. In contrast, the parental *pf14* cells had flaccid flagella and were entirely immotile.

To reveal biochemical anomalies underlying the motility phenotype, axonemes were prepared from two independent isolates for each construct. Immunoblots showed that RSP3 and LC8 in 1-5AAA axonemes were clearly less abundant than in the other axonemes of similar loads (IC140 for loading control; Fig. 9 A, arrows). To test whether AAA mutations perturbed LC8–RSP3 interactions, most LC8-containing dyneins were extracted from axonemes with NaCl, and then, the RSPs were extracted with KI. The KI extracts contained most of the RSP3 and some residual dyneins, as indicated by IC140 (Fig. 9). Immunoblots showed that unlike WT RSs, a small fraction of RSs from the two 3-5AAA mutants were extracted by NaCl (arrows in Fig. 9 B, left), suggesting that the association of 3-5AAA RSs with axonemes was less stable than WT RSs. Importantly, in 3-5AAA KI extracts, LC8 was less abundant than in the WT KI extract (arrows in Fig. 9 B, right).

Table 2. **The effect of mutations at LC8-binding motifs in the RSP3 gene on *Chlamydomonas* motility**

Strain	Motifs					Motility phenotype	Swimmers
	1 (TQT)	2 (TQTQT)	3 (IQT)	4 (TQT)	5 (TQI)		
							%
pf14						Paralyzed	0
WT						WT	95
1-2AN	ANT	TNANT				WT	96
3-5AN			INA	ANT	ANI	WT	92
1-5AN	ANT	TNANT	INA	ANT	ANI	WT	90
1-2AAA	AAA	AAAAA				WT	97
3-5AAA			AAA	AAA	AAA	Slow/twitch	∼40–60
1-5AAA	AAA	AAAAA	AAA	AAA	AAA	Slow/twitch	∼40–60

These results indicate that AAA mutations perturb the interactions between LC8 and RSP3 and the association of RSs with axonemes.

Mutations in the LC8-binding sites affected the phosphorylation of RSP3. On gradient gels, the mutated and tagged RSP3 sometimes appeared as tightly packed double bands, contrary to the single band of WT RSP3 (Fig. 9 A, right). After 6% SDS-PAGE, the RSP3 molecules from 3-5AAA, 1-5AAA, or 1-5AN strains were all clearly resolved into two bands (dot and line in Fig. 9 C, top); the lower band (Fig. 9 C, line) migrated faster than WT RSP3. The tagged RSP3 double bands from the RSP3 mutants resemble the untagged double RSP3 bands from the LC8 mutant *fla14-3* and the spoke mutant *pf27* of an unknown genetic defect (Fig. 9 C, bottom; Yang and Yang, 2006; Yang et al., 2009). The axonemes of *pf27* contain less RSs, and in vivo ^{32}P labeling showed that phosphorylation of RSP3 and the other spoke phosphoproteins was absent or diminished (Huang et al., 1981; Yang and Yang, 2006). To test for RSP3 phosphorylation in mutant axonemes, a blot of axonemes was probed with a monoclonal antibody that specifically recognized epitopes containing phospho–Thr-Pro (p-Thr-Pro), the phosphorylation site of Pro-directed protein kinases. Only two such sites are present in RSP3, both located near the TQT-like motifs (Fig. 2 B, asterisks), and the equivalent sites in human RSP3 are phosphorylated in vitro by ERK1/2 (Jivan et al., 2009). The protein loads were adjusted so that the RSP3 amount in each lane was similar, except the negative control *pf14*. The p-Thr-Pro antibody recognized the upper RSP3 band (Fig. 9 C, dot) but not the lower band (Fig. 9 C, line) in the axonemes with mutated LC8 (*fla14-3*) or mutated RSP3 (3-5AAA; compare RSP3 and p-Thr-Pro blots in Fig. 9 C, bottom). Neither band was labeled in RSP3 from *pf27*. Together, these data indicate that RSP3 is a substrate of a Pro-directed protein kinase, and one or both conserved phosphorylation sites near the LC8-binding region are hypophosphorylated as a result of mutations in LC8 or the LC8-binding sites in RSP3.

Discussion

This study demonstrates that RSP3 is an LC8-binding protein in the RS, and LC8 binding affects RSP3 and RS assembly in multiple related events. These results shed light on the process of ciliogenesis and the diverse roles of LC8 on LC8-containing complexes.

RSP3 N terminus binds to multiple LC8 dimers

Independent lines of evidence indicate that multiple LC8 dimers bind to $RSP3_{1–160}$ in tandem, but the exact number is unclear. This region contains five LC8-binding motifs (Fig. 1 A). The following lines of evidence suggest that only the last three sites bind LC8: sequence conservation of these three sites (Fig. 1 A), the 1:3 ratio of $RSP3_{1–160}$/LC8 in vitro (Fig. 3), and the lack of obvious deficiencies in 1-2AAA strains. However, we cannot rule out that the first two sites in the axoneme-binding region bind LC8, as RS deficiency in 1-5AAA strains is more severe than in 3-5AAA strains (Fig. 9 A); some LC8-binding sites do not have TQT-like sequences (Espindola et al., 2000; Lightcap et al., 2009); AAA mutations at the first two sites only may not completely block LC8 binding; and more LC8 molecules were present in the larger RS proteolytic subcomplex with the 30-kD RSP3 fragments than in the smaller one with the 20-kD RSP3

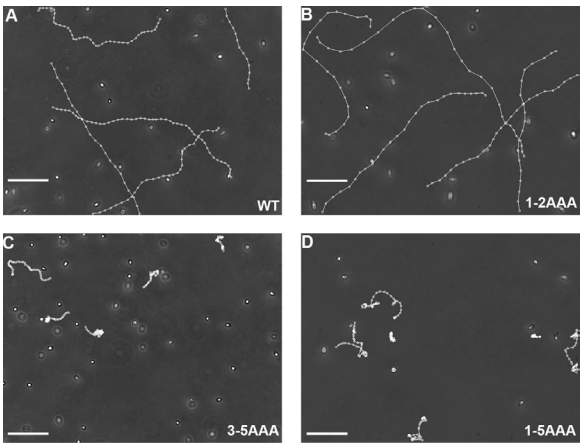

Figure 8. **The mutants defective in three to five LC8-binding motifs in RSP3 exhibit severe motility deficiencies.** (A–D) Representative recording of the liquid cultures of 1-5AAA, 3-5AAA, and 1-2AAA mutants. The videos were recorded at 200× magnification and 16 frames/s, and the motile cells were tracked using the MetaMorph program to reveal their trajectories. The tracking showed that the motile cells in the cultures of 3-5AAA and 1-5AAA strains moved slowly and locally with irregular trajectories. 1-2AAA cells swam in linear or helical trajectories as WT. Bars, 100 µm.

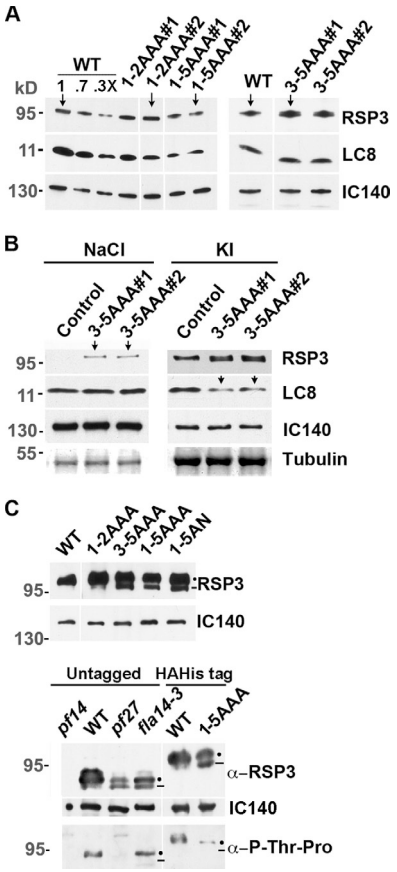

Figure 9. **The axonemes with 3-5AAA mutations are deficient in the RS, LC8, and RSP3 phosphorylation.** (A) Representative Western blots of axonemes from two mutant strains of each group, as indicated. The three lanes with decreasing amounts of WT axonemes and the blot of IC140 in I1 dynein showed protein loads. All mutated RSP3 polypeptides could be assembled into the axonemes. The amounts of RSP3 and LC8 in 1-5AAA axonemes appeared less abundant than in the others (compare arrows). (B) Western blots of the NaCl extract and the subsequent KI extract of 3-5AAA axonemes. Contrary to WT control, a fraction of the RSs from the axonemes of transformants was extracted by 0.6 M NaCl (arrows, left) along with dyneins, represented by IC140. LC8 in the KI extracts that contained most RSP3 polypeptides were less abundant in the 3-5AAA samples (arrows, right) than the WT control. (A and B) Gradient gels were used to resolve all relevant proteins. (C) Western blots of the 6% SDS-PAGE revealed hypophosphorylated RSP3 in the axonemes of RSP3 and LC8 mutants. The tagged RSP3 defective in the last three LC8-binding motifs migrates as double bands (dots and line), the lower band (line) migrating faster than the tagged RSP3 in WT control strain and 1-2AAA strain (top). Likewise, a fraction of the untagged RSP3 polypeptides in *pf27* and *fla14-3* migrated faster than the untagged WT RSP3 (bottom). In addition, RS abundance was reduced in these two mutants (compared RSP3 and IC140 blots). To probe for phosphorylation, protein loads were adjusted to make each lane, except *pf14*, contain similar amounts of RSP3. The upper RSP3 band (dot) in the RSP3 mutant or the LC8 mutant *fla14-3* was recognized by a p-Thr-Pro antibody, whereas the lower band (line) was not. In *pf27*, neither RSP3 band was recognized by the antibody.

fragments (Fig. 2). Even though the exact position of these fragments was not determined, predicted trypsin sites and varied abundance of the 30-kD fragment among preparations suggest that the 20-kD RSP3 fragment lacks the first two LC8-binding sites, which are likely present in the larger fragment. Therefore, further experiments are required to determine whether the first two LC8-binding sites of *Chlamydomonas* RSP3 are functional and present in other organisms.

Although conservative mutagenesis is sufficient to functionally perturb single LC8-binding sites in target proteins (Puthalakath et al., 1999; Bergen and Pun, 2007), in RSP3, Bassoon, p53BP1, and Nup159 (Lo et al., 2005; Stelter et al., 2007; Fejtova et al., 2009), it is necessary to generate AAA mutation or truncation in tandem-aligned TQT-like motifs. The necessity of drastic mutagenesis may be related to cooperative bindings by multiple LC8 dimers. Binding of the first dimer enhances the LC8 affinity at the adjacent site 1,000 fold (Williams, et al., 2007; Hall et al., 2009), and, therefore, modest mutagenesis in such cases may not curtail LC8 binding.

The role of multiple LC8 dimers in the spokestalk

A stack of LC8 dimers may be one eukaryotic strategy to form a rigid elongated backbone with appropriate physical properties. A stack of LC8, or LC8 like, dimers associates with several molecular scaffolds, such as Bassoon in vesicular membrane (Fejtova et al., 2009), guanylate kinase domain–associated protein at the postsynaptic density (Naisbitt et al., 2000), and ICs in dynein motor complexes (Sakato and King, 2004). EM of the Nup159–LC8 complex, a component of the nuclear pore complex, revealed a 20-nm rod composed of five tightly packed LC8 dimers despite varied aa numbers separating the LC8-binding sites in Nup159. Therefore, each $RSP3_{1–160}$ dimer with a stack of three to five LC8 dimers could account for 12–20 nm of the spoke stalk, equivalent to one third to one half of its ∼40-nm length (Fig. 10, A and B; Nicastro et al., 2005). This estimate is supported by the half-length spoke stalks present in the axonemes with $RSP3_{1–178}$ that includes all LC8-binding sites and the 18-aa AH (Fig. 10 A, AH). It also explains the shorter-than-expected stalk of the 12S RS (Diener et al., 2011), which lacks the stack of LC8 dimers (Fig. 7). The stack of LC8 dimers in Nup159 was proposed to confer the rigidity that enables the pore complex to span the nuclear membrane (Stelter et al., 2007), whereas structures of smaller complexes with only two dimers were predicted to be flexible (Williams et al., 2007; Hall et al., 2009). Although physical properties of LC8 stacks remain to be resolved, the spoke stalk is predicted to be rigid, with modest elasticity so that the RS could endure tension while intermittently coupling the central pair and the outer doublets during oscillatory beating (Warner and Satir, 1974). We envisage that the optimal stiffness is bestowed partly by the LC8 stack and is further influenced by the protruding sequences between LC8-binding sites (Fig. 10 A) and other associated proteins. The LC8 stack in the RSs of the 3-5AAA strains is likely defective, leading to pliant RSs, imprecise coupling of the outer doublet microtubules to the central pair (Yang et al., 2008), and asynchronous or paralyzed flagella (Fig. 8). The first 160-aa LC8-binding region only constitutes half of the conserved region in RSP3 that extends up to the spoke head region. This suggests that dimeric RSP3 serves as the structural scaffold of the entire RS complex (Fig. 10 B).

The role of LC8 in RSP3 phosphorylation

LC8 is tightly linked to RSP3 phosphorylation. The Thr residues near the LC8-binding sites in RSP3 are phosphorylated in vitro by a Pro-directed protein kinase ERK1/2

(Jivan et al., 2009), and the phosphorylation is perturbed by mutations in either LC8 or the last three LC8-binding motifs in RSP3 (Figs. 1 A and 9 C). This finding provides in vivo validation of the in vitro study and is consistent with the double $RSP3_{1–170}$ bands in SDS-PAGE (Fig. 5), the lower form likely being hypophosphorylated. Similarly, the faster-migrating RSP3 in LC8-free RS complexes also is likely hypophosphorylated, as seen in the 12S RS in WT membrane plus matrix (Fig. 7) and in the 20S and 12S RSs in the LC8-null *fla14* membrane plus matrix (Qin et al., 2004). In the yeast two-hybrid system, ERK1/2 binds to an N-terminal extension of a mammalian-unique, alternative, spliced RSP3 variant (Jivan et al., 2009). Perhaps ERK1/2 is tethered to this variant to enhance the efficiency of LC8-dependent phosphorylation in the flagella of selected cell types. For RSP3 molecules that lack this ERK-binding sequence, phosphorylation may rely on one of the ERK-like MAPKs or the other Pro-directed kinases found in flagellar proteome (Pazour et al., 2005).

Phosphorylation has been implicated in the regulation of flagellar beating (Piperno and Luck, 1981; Segal and Luck, 1985; Porter and Sale, 2000) and the assembly and disassembly of axonemal complexes (Qin et al., 2004; Luo et al., 2011). Although the phosphorylation of RSP3 is linked to the LC8-dependent RS assembly process, its significance remains uncertain. Hypophosphorylated RSP3 was assembled into axonemes, and RS assembly and the motility of the 1-5AN flagella with hypophosphorylated RSP3 appeared normal (Fig. 9 A). It is possible that the fraction of hypophosphorylated RSP3 in these transformants is too low to cause a phenotype. Alternatively, phosphorylation may facilitate rather than be an absolute requirement for certain molecular interactions, some of which may be dispensable. For example, phosphorylation of the two Thr residues near the LC8-binding sites may accelerate RSP3's association with the spoke-docking proteins and with the RIIa domain in RSP7 and RSP11 (Fig. 10 B, R). Or, LC8 binding, RSP3 phosphorylation, and RSP3 refolding occur synergistically, progressing toward RSP3's N terminus.

The role of LC8 in docking RSs

The collective evidence from this study and previous work strongly suggests that LC8 helps RSP3 to dock to axonemes. Bacterially expressed RSP3 could directly bind to the spokeless axoneme, but the binding was enhanced significantly by LC8 (Fig. 4). Similarly, RSP3 expressed in rabbit reticulocyte lysate binds to *pf14* axonemes specifically (Diener et al., 1993), likely with the help of the highly conserved and ubiquitous LC8 (Pfister et al., 2006) in the lysate. These results could explain the absence of RSs in the LC8-null axonemes (Fig. 9 A; Pazour et al., 1998) despite the presence of 12S RS precursors and 20S mature RSs in the flagella (Qin et al., 2004). Presumably, without LC8, the RS cannot dock efficiently to the axoneme. The fact that LC8 is undetectable in purified 12S RS complexes (Fig. 7) in spite of seemingly copious LC8 molecules in the flagellar matrix and the cell body (Puthalakath et al., 1999; Rompolas et al., 2007) suggests that RSP3 does not have access to LC8 until RSP3 is ready to interact with docking

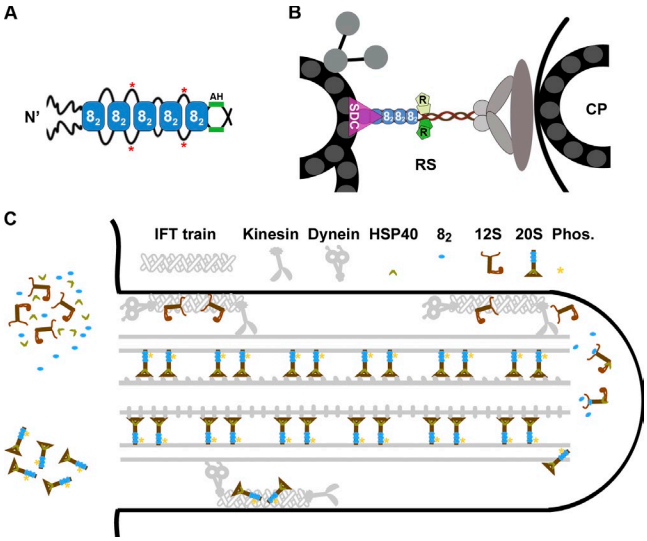

Figure 10. **Models depicting the effects of LC8 on the RS complex.** (A) Multiple LC8 dimers (blue rectangles, 8_2) associate with a dimeric RSP3 (black lines) at the region N terminal (N') upstream of the AH. The sequences between the LC8-binding sites may loop out of the stack and become phosphorylated (red asterisks). (B) The dimeric RSP3 N terminus and the stack of LC8 form the basal part of the RS. Phosphorylation near the LC8-binding sites may alter local conformation, promoting the interactions of the nearby AH with homodimeric RIIa domains (R) and the interaction of the axonemal binding region with the spoke-docking complex (SDC), possibly the CSC, or a FAP206-containing complex. Only a fraction of the 9 + 2 axoneme and relevant RSPs are illustrated. CP, central pair. (C) The two-stage assembly process of the RS complex in the cell body (left) and flagellum (right). LC8 dimer and HSP40 dimer do not join the RS until the L-shaped 12S RS precursors are transported into flagella by kinesin-driven IFT. Association of HSP40 with the 12S RS transforms the spokehead, whereas binding of LC8 to the N-terminal region of RSP3 in the 12S RS triggers formation of the stalk base, phosphorylation (Phos.) of RSP3 (asterisks), and docking of the T-shaped 20S RS to the axoneme. The unbound 20S RSs are delivered back to the cell body by dynein-driven IFT. The unknown transport mechanisms of LC8 and HSP40 are not depicted.

proteins, perhaps at the tip of flagella, where RSs are added to growing axonemes (Johnson and Rosenbaum, 1992).

RSP3 may associate with two distinct spoke-docking complexes. Although the CSC is implicated in docking only the second RS in each 96-nm repeat (Dymek and Smith, 2007; Dymek et al., 2011), the $RSP3_{1–178}$ pull-down contains LC8, the CSC (Fig. 6), and, interestingly, FAP206 as well. FAP206 does not seem to be copurified with the CSC or the RS (Dymek and Smith, 2007) but is linked to RS assembly. It is less abundant in the spokeless axonemes, and, like the CSC, FAP206 is reduced or phosphorylated differently in the mutant axonemes defective in the nexin–dynein regulatory complex (N-DRC; Lin et al., 2011). One interesting scenario is that FAP206 and the CSC are respectively involved in docking spoke 1 and spoke 2 to distinct parts of the N-DRC that links the two RSs, functionally and structurally, to distinct inner dynein species (Huang et al., 1981; Piperno et al., 1992; Porter and Sale, 2000; Kamiya, 2002; Nicastro et al., 2005; Heuser, et al., 2009; Pigino et al., 2011). Intriguingly, CaM copurifies with the CSC from the axonemal extracts of various strains except the N-DRC mutants (Dymek and Smith, 2007) and the $RSP3_{1–178}$ strain (Fig. 6 A). The integrity of N-DRC and the RS may affect association of CaM with the CSC.

In conclusion, we propose an RS assembly model as follows: LC8 and the 12S precursors enter flagella separately (Fig. 10 C). Upon arrival at the tip of the flagella, the N-terminal region of RSP3 in the 12S RS precursor becomes accessible to LC8 dimers, and the synergistic binding of multiple LC8 dimers triggers a series of events: the formation of a stack of LC8 dimers as the basal part of the stalk, RSP3 phosphorylation to promote further molecular interactions, and the interaction of RSP3 with two sets of docking proteins, integrating RSs into elongating axonemes. This model explains the requirement of RSP3 sequences beyond the LC8-binding and axoneme-docking region for substantial RS assembly (Fig. 5) and the susceptibility of RS assembly to the additional 23-aa tail of LC8 in *fla14-3*. The extended tail sticking out at the stacking interface (Liang et al., 1999) could impede stacking and the downstream molecular interactions, resulting in unstable RSs of reduced abundance and hypophosphorylated RSP3 (Yang et al., 2009). These multiple impacts from the LC8 dimer could be attributed entirely to its ability to bind and meanwhile refold dimeric polypeptide chains (Barbar, 2008). In this sense, the LC8 dimer operates as molecular glue as well as a chaperone. Interestingly, other two chaperones, spoke HSP40 (Yang et al., 2006) and HSP70 (Bloch and Johnson, 1995), are also implicated in the final assembly process at the tip of flagella. Perhaps chaperones and phosphoenzymes work concertedly at the tip to transform various precursor complexes into the precise axonemal supercomplex.

Materials and methods

Strains and culture

The *Chlamydomonas reinhardtii* strains used in this work included the following: CC-124 (WT), *pf14* (lacking RSs), *fla14-1* (LC8-null mutant), *fla14-3* (LC8 read-through mutant), *pf27* (with hypophosphorylation and reduced amounts of RSs), and *pf28pf30* (lacking outer dynein arms and I1 inner dynein). They were obtained from the *Chlamydomonas* Resource Center (Harris, 2001). Cells were cultured in Tris-acetate-phosphate medium with aeration on a 14/10-h light/dark cycle (Yang et al., 2009).

Molecular biology

Bacterial expression constructs. The S-tagged $RSP3_{1–160}$ construct was generated by PCR amplification using a GST-RSP3 cDNA construct (Diener et al., 1993) as a template and primers with built-in BglII and XhoI restriction sites. The PCR product was cloned in frame into pET Duet-1 vector (EMD) to produce RSP3 with a C-terminal S tag. The His-tagged LC8 construct was generated by PCR amplification using an LC8 cDNA clone (Yang et al. 2009) as a template and primers with built-in NdeI and EcoRI restriction sites. The PCR fragment was cloned into the pET28-(a) vector (EMD) in frame to express LC8 with a 6-His tag at the N terminus. These expression constructs were transformed into *Escherichia coli* strain BL21(DE3). Expression was induced with 1 mM IPTG at 18°C overnight.

***Chlamydomonas* transformation constructs.** An NcoI fragment containing the RSP3 genomic sequence was released from a BAC clone and inserted into pGEM-T Easy vector (Promega). To aid cloning, the SacI site and its downstream sequence at the 3′ flanking region were eliminated by limited restriction digest followed by treatment with T4 DNA polymerase. To add a tag with three HA epitopes and 12 His residues, PCR was performed using modified primers to first add an XhoI site, six His codons before the endogenous stop codon, and an XbaI site after the stop codon. Subsequently, a PCR fragment encoding three HA and six His codons was inserted into the XhoI site. For single-plasmid transformation, the paromomycin (PMM) expression cassette was amplified from pSI103 (Yang et al., 2009) and inserted into the AatII site in the vector. The final plasmid was named pPMM-RSP3-HAHis.

For site-directed mutagenesis, the region of RSP3 containing the LC8-binding motifs flanked by two SpeI sites was PCR amplified. The second SpeI site was replaced with XbaI, an isoschizomer, for cloning purposes. The PCR product was cloned into pGEM-T Easy vector. This construct, with only an 831-bp insert, was used as a template to generate point mutations using the QuikChange strategy (Agilent Technologies). Mutation was confirmed by sequencing. The mutated SpeI–XbaI fragment was used to replace the WT SpeI–SpeI fragment in pPMM-RSP3-HAHis. The clones were analyzed by an SpeI digest, which linearized the mutant construct but released the SpeI fragment from the parental construct.

For the $RSP3_{1–170}$-Cys truncation construct, the sequence for the N-terminal 170 aa and the 3′ untranslated region including the flanking sequence were PCR amplified using primers with built-in EcoRI and XbaI sites. The two PCR products were ligated and cloned into the EcoRI site in pGEM-T. As $RSP3_{1–170}$ was unlikely to restore motility to *pf14* cells (Diener et al., 1993), a PMM-resistant cassette was inserted into the vector to identify the transformants. The ligation at the XbaI site eliminated the endogenous stop codon in the RSP3 gene, resulting in the translation of 23 aa, including three Cys residues, encoded by the 3′ untranslated region. A PCR product encoding three HA and 12 His codon was cloned into the XbaI site to generate the p$RSP3_{1–170}$-HAHis construct.

Transformation

For single-plasmid transformation, the glass beads method was used to introduce individual RSP3 genomic constructs carrying a PMM selection cassette into the RSP3 mutant *pf14* (Kindle, 1990; Diener et al., 1993). The cells were then plated on Tris-acetate-phosphate plates supplemented with 10 µg/ml PMM for selection. After 4 d, a fraction of each surviving clone was suspended in water for microscopic observations. Crude flagella were prepared from 10 antibiotic-resistant clones for Western blots to identify RSP3/HA-positive clones.

Biochemistry

Axoneme preparation and serial extraction. Flagella were isolated by the dibucaine method (Yang et al., 2001). For axoneme preparation, the isolated flagella were demembranated by 0.5% NP-40 in buffer A (10 mM Hepes, pH 7.2, 5 mM $MgSO_4$, 1 mM DTT, 0.5 mM EDTA, and 30 mM NaCl) supplemented with protease inhibitors, 0.1 mM PMSF, and 0.5 trypsin inhibitor U/ml aprotinin. Axonemes were suspended in 0.6 M NaCl/buffer A at 2–5 mg protein/ml on ice for 30 min. After incubation, the suspension was centrifuged at 12,000 rpm for 10 min in a TA-15 rotor (Beckman Coulter). The supernatant contained dyneins. For RS extraction, the pellet after the NaCl extraction was resuspended in buffer A containing 0.6 M KI. After incubation on ice for 30 min, centrifugation was performed at 12,000 rpm for 10 min to obtain the supernatant containing RSs.

Limited proteolysis. The *pf28pf30* axonemes were isolated as described in the previous paragraph, except that DTT, EDTA, EGTA, PMSF, and aprotinin were omitted throughout the experiments. The axonemal pellet was resuspended in buffer A at a concentration of 2 mg/ml and treated with trypsin at different concentrations for 40 min at room temperature. The digestion was terminated by the addition of an excess of trypsin inhibitor (Summers and Gibbons, 1971).

Analysis of trypsin-treated axonemes. The trypsin-treated axonemes were extracted with 0.6 M KI/buffer A. After dialysis against buffer A and centrifugation, Laemmli sample buffer for standard SDS-PAGE was added to the supernatant. Identical procedures were performed for electrophoresis with 6% native gels, except that SDS was excluded. For the 2D analysis, native gel strips were equilibrated in 5× SDS sample buffer at room temperature for 1 h. Each strip was then inserted onto a (6–16%) gradient gel for SDS-PAGE. The proteins in the SDS or native gels were transferred to nitrocellulose membranes followed by Western blot analysis.

Affinity purification. For purification of recombinant $RSP3_{1–160}$–S tag and His-tagged LC8, bacteria were harvested from the IPTG-induced overnight culture, and the cell suspension was sonicated followed by centrifugation at 12,000 rpm. The supernatant was subjected to affinity purification with S agarose (EMD) or Ni-NTA (QIAGEN) following procedures recommended by the manufacturers. The interaction of $RSP3_{1–160}$ and His-LC8 was assessed by Ni-NTA purification after the incubation of equal or different volumes of the two bacterial extracts containing each protein for 1 h at room temperature. The samples were fractionated in SDS-PAGE and stained with Coomassie blue. The mean density of $RSP3_{1–160}$ and His-LC8 bands in the pull-down was quantified using a gel documentation system (UVP, LLC). Various amounts of the pull-down were analyzed to ensure that the protein load and stain were within the linear range for densitometry.

For purification of truncated tagged spoke complexes, the axonemes from the $RSP3_{1–178}$-HAHis strain or control *pf14* were extracted with 0.6 M KI/buffer A at a protein concentration of 5 mg/ml. The extracts were

diluted to 0.3 M KI with 10 mM imidazole buffer. The supernatant was subjected to Ni-NTA purification.

In vitro reconstitution. Equal amounts of bacterial extracts containing S-tagged $RSP3_{1–160}$ and His-LC8 were added into different amounts of *pf14* or WT axonemes. After a 1-h incubation at room temperature, the axonemes were spun down at 8,000 rpm for 10 min. The pellets were washed with 150 mM NaCl/buffer A and then resuspended in Laemmli sample buffer for Western blot analysis.

Analysis of LC8 in the spoke complexes. Flagella were isolated from *pf28 pf30* cells by pH shock and subjected to two cycles of freeze/thaw. The axonemes were sedimented at 14,000 *g*, and the supernatant was clarified at 100,000 *g* for 15 min. The supernatant was loaded onto three 12-ml 10–30% sucrose gradients and was centrifuged at 38,000 rpm for 18 h in an SW41 rotor (Beckman Coulter). The 12S and 20S RS complexes were identified on Coomassie blue–stained gels of gradient fractions. Fractions containing the 12S or 20S complex were pooled, brought up to 300 mM NaCl, and loaded onto a 1-ml MonoQ column (GE Healthcare). Proteins were eluted with a 16-ml NaCl gradient, 300–650 mM for the 20S complex, and 300–600 mM for the 12S complex. The complexes were identified on silver-stained gels of the elution fractions. After dialysis to remove the NaCl, the peak 20S and 12S fractions were analyzed on immunoblots probed with antibodies against RSP3 and LC8.

Chemical cross-linking. Axonemes prepared in DTT-free buffer A at a concentration of 2 mg/ml were treated with EDC HCl (Thermo Fisher Scientific) at a series of concentrations for 1 h at room temperature. The reaction of ∼40 µl was terminated by adding Laemmli sample buffer and 1 µl β–mercaptoethanol.

Antibodies. The monospecific antibodies used in this study recognized p28 (provided by G. Piperno, Mount Sinai Medical School, New York, NY), IC140 (provided by W.S. Sale, Emory University, Atlanta, GA), CaM, IP2, and IP3 (provided by E.F. Smith, Dartmouth College, Hanover, NH), HA (Covance), and RSP2, RSP3, LC8, and RSP11 (Yang and Yang, 2006). The pan-RSP3 rabbit antibody was raised against the affinity-purified 418-aa isoform of recombinant human RSP3. p-Thr's were probed with a p-Thr-Pro mouse monoclonal antibody following the instructions of the manufacturer (Cell Signaling Technology).

Motility analysis

For screening transformants, 30-µl aliquots of log-phase cultures were observed under a compound microscope (BH-2; Olympus) upon the fluid flow cessation. The estimated percentage of swimmers was derived from the numbers of swimmers divided by the total cells in the field (Yang and Yang, 2006). The cells stuck to the glass were not counted. For trajectory analysis, images were captured using a compound microscope (Eclipse E600W; Nikon) and a digital monochrome charge-coupled device camera (CoolSNAP ES; Photometrics) at a 16/s frame rate. Swimming trajectories were tracked with MetaMorph software (Molecular Devices). All microscopy was conducted at room temperature using 20× Plan Fluor objective lenses with an NA of 0.4 or 0.5.

Sequence analysis

The RSP3 homologs were identified by a BLASTP search against the protein database. ClustalW (1.83) was used to generate multiple sequence alignment of RSP3 homologs. The Jpred program was used for secondary structure prediction. Regional disorder in the tertiary structure was predicted using the Regional Order Neural Network.

We wish to thanks Dr. Elizabeth F. Smith for providing antibodies and Dr. James Courtright (Marquette University, Milwaukee, WI) for the development of the TQT sequence screening program and critical advice on the manuscript.

This work is supported by grants from the National Institutes of Health (GM14642 to J.L. Rosenbaum and GM090162 to P. Yang).

Submitted: 8 November 2011
Accepted: 5 June 2012

References

Barbar, E. 2008. Dynein light chain LC8 is a dimerization hub essential in diverse protein networks. *Biochemistry*. 47:503–508. http://dx.doi.org/10.1021/bi701995m

Bergen, J.M., and S.H. Pun. 2007. Evaluation of an LC8-binding peptide for the attachment of artificial cargo to dynein. *Mol. Pharm.* 4:119–128. http://dx.doi.org/10.1021/mp060086o

Bloch, M.A., and K.A. Johnson. 1995. Identification of a molecular chaperone in the eukaryotic flagellum and its localization to the site of microtubule assembly. *J. Cell Sci.* 108:3541–3545.

DiBella, L.M., O. Gorbatyuk, M. Sakato, K. Wakabayashi, R.S. Patel-King, G.J. Pazour, G.B. Witman, and S.M. King. 2005. Differential light chain assembly influences outer arm dynein motor function. *Mol. Biol. Cell*. 16:5661–5674. http://dx.doi.org/10.1091/mbc.E05-08-0732

Diener, D.R., L.H. Ang, and J.L. Rosenbaum. 1993. Assembly of flagellar radial spoke proteins in *Chlamydomonas*: Identification of the axoneme binding domain of radial spoke protein 3. *J. Cell Biol.* 123:183–190. http://dx.doi.org/10.1083/jcb.123.1.183

Diener, D.R., P. Yang, S. Geimer, D.G. Cole, W.S. Sale, and J.L. Rosenbaum. 2011. Sequential assembly of flagellar radial spokes. *Cytoskeleton (Hoboken)*. 68:389–400.

Dymek, E.E., and E.F. Smith. 2007. A conserved CaM- and radial spoke–associated complex mediates regulation of flagellar dynein activity. *J. Cell Biol.* 179:515–526. http://dx.doi.org/10.1083/jcb.200703107

Dymek, E.E., T. Heuser, D. Nicastro, and E.F. Smith. 2011. The CSC is required for complete radial spoke assembly and wild-type ciliary motility. *Mol. Biol. Cell*. 22:2520–2531. http://dx.doi.org/10.1091/mbc.E11-03-0271

Espindola, F.S., D.M. Suter, L.B. Partata, T. Cao, J.S. Wolenski, R.E. Cheney, S.M. King, and M.S. Mooseker. 2000. The light chain composition of chicken brain myosin-Va: Calmodulin, myosin-II essential light chains, and 8-kDa dynein light chain/PIN. *Cell Motil. Cytoskeleton*. 47:269–281. http://dx.doi.org/10.1002/1097-0169(200012)47:4<269::AID-CM2>3.0.CO;2-G

Fejtova, A., D. Davydova, F. Bischof, V. Lazarevic, W.D. Altrock, S. Romorini, C. Schöne, W. Zuschratter, M.R. Kreutz, C.C. Garner, et al. 2009. Dynein light chain regulates axonal trafficking and synaptic levels of Bassoon. *J. Cell Biol.* 185:341–355. http://dx.doi.org/10.1083/jcb.200807155

Gaillard, A.R., L.A. Fox, J.M. Rhea, B. Craige, and W.S. Sale. 2006. Disruption of the A-kinase anchoring domain in flagellar radial spoke protein 3 results in unregulated axonemal cAMP-dependent protein kinase activity and abnormal flagellar motility. *Mol. Biol. Cell*. 17:2626–2635. http://dx.doi.org/10.1091/mbc.E06-02-0095

Hall, J., P.A. Karplus, and E. Barbar. 2009. Multivalency in the assembly of intrinsically disordered dynein intermediate chain. *J. Biol. Chem.* 284:33115–33121. http://dx.doi.org/10.1074/jbc.M109.048587

Harris, E.H. 2001. *Chlamydomonas* as a model organism. *Annu. Rev. Plant Physiol. Plant Mol. Biol.* 52:363–406. http://dx.doi.org/10.1146/annurev.arplant.52.1.363

Heuser, T., M. Raytchev, J. Krell, M.E. Porter, and D. Nicastro. 2009. The dynein regulatory complex is the nexin link and a major regulatory node in cilia and flagella. *J. Cell Biol.* 187:921–933. http://dx.doi.org/10.1083/jcb.200908067

Huang, B., G. Piperno, Z. Ramanis, and D.J. Luck. 1981. Radial spokes of *Chlamydomonas* flagella: Genetic analysis of assembly and function. *J. Cell Biol.* 88:80–88. http://dx.doi.org/10.1083/jcb.88.1.80

Jaffrey, S.R., and S.H. Snyder. 1996. PIN: An associated protein inhibitor of neuronal nitric oxide synthase. *Science*. 274:774–777. http://dx.doi.org/10.1126/science.274.5288.774

Jivan, A., S. Earnest, Y.C. Juang, and M.H. Cobb. 2009. Radial spoke protein 3 is a mammalian protein kinase A-anchoring protein that binds ERK1/2. *J. Biol. Chem.* 284:29437–29445. http://dx.doi.org/10.1074/jbc.M109.048181

Johnson, K.A., and J.L. Rosenbaum. 1992. Polarity of flagellar assembly in *Chlamydomonas*. *J. Cell Biol.* 119:1605–1611. http://dx.doi.org/10.1083/jcb.119.6.1605

Kamiya, R. 2002. Functional diversity of axonemal dyneins as studied in *Chlamydomonas* mutants. *Int. Rev. Cytol.* 219:115–155. http://dx.doi.org/10.1016/S0074-7696(02)19012-7

Kindle, K.L. 1990. High-frequency nuclear transformation of *Chlamydomonas reinhardtii*. *Proc. Natl. Acad. Sci. USA*. 87:1228–1232. http://dx.doi.org/10.1073/pnas.87.3.1228

King, S.M., and R.S. Patel-King. 1995. The M(r) = 8,000 and 11,000 outer arm dynein light chains from *Chlamydomonas* flagella have cytoplasmic homologues. *J. Biol. Chem.* 270:11445–11452. http://dx.doi.org/10.1074/jbc.270.19.11445

LeDizet, M., and G. Piperno. 1995. The light chain p28 associates with a subset of inner dynein arm heavy chains in *Chlamydomonas* axonemes. *Mol. Biol. Cell*. 6:697–711.

Liang, J., S.R. Jaffrey, W. Guo, S.H. Snyder, and J. Clardy. 1999. Structure of the PIN/LC8 dimer with a bound peptide. *Nat. Struct. Biol.* 6:735–740. http://dx.doi.org/10.1038/11501

Lightcap, C.M., G. Kari, L.E. Arias-Romero, J. Chernoff, U. Rodeck, and J.C. Williams. 2009. Interaction with LC8 is required for Pak1 nuclear import

and is indispensable for zebrafish development. *PLoS ONE*. 4:e6025. http://dx.doi.org/10.1371/journal.pone.0006025

Lin, J., D. Tritschler, K. Song, C.F. Barber, J.S. Cobb, M.E. Porter, and D. Nicastro. 2011. Building blocks of the nexin-dynein regulatory complex in *Chlamydomonas* flagella. *J. Biol. Chem.* 286:29175–29191. http://dx.doi.org/10.1074/jbc.M111.241760

Lo, K.W., S. Naisbitt, J.S. Fan, M. Sheng, and M. Zhang. 2001. The 8-kDa dynein light chain binds to its targets via a conserved (K/R)XTQT motif. *J. Biol. Chem.* 276:14059–14066. http://dx.doi.org/10.1074/jbc.M104701200

Lo, K.W., H.M. Kan, L.N. Chan, W.G. Xu, K.P. Wang, Z. Wu, M. Sheng, and M. Zhang. 2005. The 8-kDa dynein light chain binds to p53-binding protein 1 and mediates DNA damage-induced p53 nuclear accumulation. *J. Biol. Chem.* 280:8172–8179. http://dx.doi.org/10.1074/jbc.M411408200

Luo, M., M. Cao, Y. Kan, G. Li, W. Snell, and J. Pan. 2011. The phosphorylation state of an aurora-like kinase marks the length of growing flagella in *Chlamydomonas*. *Curr. Biol.* 21:586–591. http://dx.doi.org/10.1016/j.cub.2011.02.046

Naisbitt, S., J. Valtschanoff, D.W. Allison, C. Sala, E. Kim, A.M. Craig, R.J. Weinberg, and M. Sheng. 2000. Interaction of the postsynaptic density-95/guanylate kinase domain-associated protein complex with a light chain of myosin-V and dynein. *J. Neurosci.* 20:4524–4534.

Navarro-Lérida, I., M. Martínez Moreno, F. Roncal, F. Gavilanes, J.P. Albar, and I. Rodríguez-Crespo. 2004. Proteomic identification of brain proteins that interact with dynein light chain LC8. *Proteomics*. 4:339–346. http://dx.doi.org/10.1002/pmic.200300528

Nicastro, D., J.R. McIntosh, and W. Baumeister. 2005. 3D structure of eukaryotic flagella in a quiescent state revealed by cryo-electron tomography. *Proc. Natl. Acad. Sci. USA*. 102:15889–15894. http://dx.doi.org/10.1073/pnas.0508274102

Patel-King, R.S., O. Gorbatyuk, S. Takebe, and S.M. King. 2004. Flagellar radial spokes contain a Ca2+-stimulated nucleoside diphosphate kinase. *Mol. Biol. Cell*. 15:3891–3902. http://dx.doi.org/10.1091/mbc.E04-04-0352

Pazour, G.J., C.G. Wilkerson, and G.B. Witman. 1998. A dynein light chain is essential for the retrograde particle movement of intraflagellar transport (IFT). *J. Cell Biol.* 141:979–992. http://dx.doi.org/10.1083/jcb.141.4.979

Pazour, G.J., N. Agrin, J. Leszyk, and G.B. Witman. 2005. Proteomic analysis of a eukaryotic cilium. *J. Cell Biol.* 170:103–113. http://dx.doi.org/10.1083/jcb.200504008

Pfister, K.K., P.R. Shah, H. Hummerich, A. Russ, J. Cotton, A.A. Annuar, S.M. King, and E.M. Fisher. 2006. Genetic analysis of the cytoplasmic dynein subunit families. *PLoS Genet.* 2:e1. http://dx.doi.org/10.1371/journal.pgen.0020001

Pigino, G., K.H. Bui, A. Maheshwari, P. Lupetti, D. Diener, and T. Ishikawa. 2011. Cryoelectron tomography of radial spokes in cilia and flagella. *J. Cell Biol.* 195:673–687. http://dx.doi.org/10.1083/jcb.201106125

Piperno, G., and D.J. Luck. 1981. Inner arm dyneins from flagella of *Chlamydomonas reinhardtii*. *Cell*. 27:331–340. http://dx.doi.org/10.1016/0092-8674(81)90416-5

Piperno, G., K. Mead, and W. Shestak. 1992. The inner dynein arms I2 interact with a "dynein regulatory complex" in *Chlamydomonas* flagella. *J. Cell Biol.* 118:1455–1463. http://dx.doi.org/10.1083/jcb.118.6.1455

Porter, M.E., and W.S. Sale. 2000. The 9 + 2 axoneme anchors multiple inner arm dyneins and a network of kinases and phosphatases that control motility. *J. Cell Biol.* 151:F37–F42. http://dx.doi.org/10.1083/jcb.151.5.F37

Puthalakath, H., D.C. Huang, L.A. O'Reilly, S.M. King, and A. Strasser. 1999. The proapoptotic activity of the Bcl-2 family member Bim is regulated by interaction with the dynein motor complex. *Mol. Cell*. 3:287–296. http://dx.doi.org/10.1016/S1097-2765(00)80456-6

Qin, H., D.R. Diener, S. Geimer, D.G. Cole, and J.L. Rosenbaum. 2004. Intraflagellar transport (IFT) cargo: IFT transports flagellar precursors to the tip and turnover products to the cell body. *J. Cell Biol.* 164:255–266. http://dx.doi.org/10.1083/jcb.200308132

Rodríguez-Crespo, I., B. Yélamos, F. Roncal, J.P. Albar, P.R. Ortiz de Montellano, and F. Gavilanes. 2001. Identification of novel cellular proteins that bind to the LC8 dynein light chain using a pepscan technique. *FEBS Lett.* 503:135–141. http://dx.doi.org/10.1016/S0014-5793(01)02718-1

Rompolas, P., L.B. Pedersen, R.S. Patel-King, and S.M. King. 2007. *Chlamydomonas* FAP133 is a dynein intermediate chain associated with the retrograde intraflagellar transport motor. *J. Cell Sci.* 120:3653–3665. http://dx.doi.org/10.1242/jcs.012773

Sakato, M., and S.M. King. 2004. Design and regulation of the AAA+ microtubule motor dynein. *J. Struct. Biol.* 146:58–71. http://dx.doi.org/10.1016/j.jsb.2003.09.026

Segal, R.A., and D.J. Luck. 1985. Phosphorylation in isolated *Chlamydomonas* axonemes: A phosphoprotein may mediate the Ca2+-dependent photophobic response. *J. Cell Biol.* 101:1702–1712. http://dx.doi.org/10.1083/jcb.101.5.1702

Stelter, P., R. Kunze, D. Flemming, D. Höpfner, M. Diepholz, P. Philippsen, B. Böttcher, and E. Hurt. 2007. Molecular basis for the functional interaction of dynein light chain with the nuclear-pore complex. *Nat. Cell Biol.* 9:788–796. http://dx.doi.org/10.1038/ncb1604

Summers, K.E., and I.R. Gibbons. 1971. Adenosine triphosphate-induced sliding of tubules in trypsin-treated flagella of sea-urchin sperm. *Proc. Natl. Acad. Sci. USA*. 68:3092–3096. http://dx.doi.org/10.1073/pnas.68.12.3092

Tan, G.S., M.A. Preuss, J.C. Williams, and M.J. Schnell. 2007. The dynein light chain 8 binding motif of rabies virus phosphoprotein promotes efficient viral transcription. *Proc. Natl. Acad. Sci. USA*. 104:7229–7234. http://dx.doi.org/10.1073/pnas.0701397104

Warner, F.D., and P. Satir. 1974. The structural basis of ciliary bend formation. Radial spoke positional changes accompanying microtubule sliding. *J. Cell Biol.* 63:35–63. http://dx.doi.org/10.1083/jcb.63.1.35

Wei, M., P. Sivadas, H.A. Owen, D.R. Mitchell, and P. Yang. 2010. *Chlamydomonas* mutants display reversible deficiencies in flagellar beating and axonemal assembly. *Cytoskeleton (Hoboken)*. 67:71–80. http://dx.doi.org/10.1002/cm.20422

Williams, J.C., P.L. Roulhac, A.G. Roy, R.B. Vallee, M.C. Fitzgerald, and W.A. Hendrickson. 2007. Structural and thermodynamic characterization of a cytoplasmic dynein light chain-intermediate chain complex. *Proc. Natl. Acad. Sci. USA*. 104:10028–10033. http://dx.doi.org/10.1073/pnas.0703614104

Wirschell, M., F. Zhao, C. Yang, P. Yang, D. Diener, A. Gaillard, J.L. Rosenbaum, and W.S. Sale. 2008. Building a radial spoke: Flagellar radial spoke protein 3 (RSP3) is a dimer. *Cell Motil. Cytoskeleton*. 65:238–248. http://dx.doi.org/10.1002/cm.20257

Yang, C., and P. Yang. 2006. The flagellar motility of *Chlamydomonas* pf25 mutant lacking an AKAP-binding protein is overtly sensitive to medium conditions. *Mol. Biol. Cell*. 17:227–238. http://dx.doi.org/10.1091/mbc.E05-07-0630

Yang, C., H.A. Owen, and P. Yang. 2008. Dimeric heat shock protein 40 binds radial spokes for generating coupled power strokes and recovery strokes of 9 + 2 flagella. *J. Cell Biol.* 180:403–415. http://dx.doi.org/10.1083/jcb.200705069

Yang, P., D.R. Diener, J.L. Rosenbaum, and W.S. Sale. 2001. Localization of calmodulin and dynein light chain LC8 in flagellar radial spokes. *J. Cell Biol.* 153:1315–1326. http://dx.doi.org/10.1083/jcb.153.6.1315

Yang, P., D.R. Diener, C. Yang, T. Kohno, G.J. Pazour, J.M. Dienes, N.S. Agrin, S.M. King, W.S. Sale, R. Kamiya, et al. 2006. Radial spoke proteins of *Chlamydomonas* flagella. *J. Cell Sci.* 119:1165–1174. http://dx.doi.org/10.1242/jcs.02811

Yang, P., C. Yang, M. Wirschell, and S. Davis. 2009. Novel LC8 mutations have disparate effects on the assembly and stability of flagellar complexes. *J. Biol. Chem.* 284:31412–31421. http://dx.doi.org/10.1074/jbc.M109.050666